frontiers | Frontiers in Neuroscience

TYPE Original Research
PUBLISHED 13 August 2025
DOI 10.3389/fnins.2025.1634582

OPEN ACCESS

EDITED BY
Jit Muthuswamy,
Arizona State University, United States

REVIEWED BY
Massoud Khraiche,
American University of Beirut, Lebanon
Melanie Ecker,
University of North Texas, United States

*CORRESPONDENCE
Ikuro Suzuki
✉ i-suzuki@tohtech.ac.jp

RECEIVED 24 May 2025
ACCEPTED 24 July 2025
PUBLISHED 13 August 2025

CITATION
Yokoi R, Matsuda N, Ishibashi Y and Suzuki I (2025) Advanced neural activity mapping in brain organoids via field potential imaging with ultra-high-density CMOS microelectrode arrays.
Front. Neurosci. 19:1634582.
doi: 10.3389/fnins.2025.1634582

Advanced neural activity mapping in brain organoids via field potential imaging with ultra-high-density CMOS microelectrode arrays

Remi Yokoi, Naoki Matsuda, Yuto Ishibashi and Ikuro Suzuki*

Department of Electronics, Graduate School of Engineering, Tohoku Institute of Technology, Sendai, Japan

Introduction: Human iPSC-derived brain organoids and assembloids have emerged as promising in vitro models for recapitulating human brain development, neurological disorders, and drug responses. However, detailed analysis of their electrophysiological properties requires advanced measurement techniques.

Methods: Here, we present an analytical approach using ultra-high-density (UHD) CMOS microelectrode arrays (MEAs) with 236,880 electrodes across a 32.45 mm2 sensing area, enabling large-scale field potential imaging (FPI) of brain organoids.

Results: Neuronal activity was recorded from over 46,000 electrodes, allowing single-cell spike detection and network connectivity analysis. In midbrain organoids, L-DOPA administration elicited both excitatory and inhibitory responses, with a dose-dependent shift toward network enhancement. Leveraging the spatiotemporal resolution of the UHD-CMOSMEA, we introduced two novel endpoints: propagation velocity and propagation area. In cortical organoids, picrotoxin increased propagation velocity, while MK-801 reduced propagation area. FPI also enabled frequency-domain analyses, revealing region-specific activity, including distinct gamma-band patterns. In midbrain–striatal assembloids, 4-aminopyridine enhanced interorganoid connectivity.

Conclusion: This single-cell-resolved, large-scale recording approach using UHD-CMOS MEAs enables detailed analysis of network connectivity, propagation dynamics, and frequency features. It provides a powerful platform for studying brain organoids and assembloids, with strong potential for drug discovery and disease modeling in human neuroscience.

KEYWORDS

UHD-CMOS-MEA, brain organoid, field potential imaging, assembloid, single neuron, network connectivity analysis, propagation velocity, propagation area

1 Introduction

The human brain exhibits remarkably complex structures and functions, and the diverse dynamics of neural activity are intricately involved in development, cognition, and disease. Brain organoids have recently attracted attention as *in vitro* models that enable the reconstruction and analysis of these brain functions. They are three-dimensional cultured tissues derived from pluripotent stem cells that self-organize into neural structures (Lancaster et al., 2013; Lancaster and Knoblich, 2014; Giandomenico et al., 2021). To date, region-specific brain organoids mimicking the cerebral cortex (Lancaster et al., 2013), striatum (Miura et al., 2020), midbrain (Jo et al., 2016), and hippocampus (Sakaguchi et al., 2015) have been developed, allowing for the recapitulation of developmental processes and functional assessment of neural networks. In the context of compound screening, brain organoids are expected to serve as novel platforms that enable more precise prediction and evaluation of drug efficacy and toxicity than conventional two-dimensional cultures or animal models. Furthermore, because brain organoids can be generated from patient-derived induced pluripotent stem cells (iPSCs), they provide an opportunity to model human-specific disease phenotypes that are difficult to reproduce in animal systems. Indeed, various disease-related features have been reported using brain organoids, including amyloid-β and tau pathology in Alzheimer's disease (Raja et al., 2016; Gonzalez et al., 2018; Yan et al., 2018), overproduction of GABAergic neurons in autism spectrum disorder (Mariani et al., 2015), reduced neural and increased neurovascular cell populations in schizophrenia (Notaras et al., 2022), and disease-specific frequency characteristics and responses to contraindicated drugs in Dravet syndrome (Yokoi et al., 2023).

To construct more structurally complex in vitro models, increasing efforts have been directed toward generating assembloids by fusing organoids derived from different brain regions. Various types of assembloids have been developed to date, including cortical–striatal (Miura et al., 2020), midbrain–striatal (Ozgun et al., 2024), and midbrain–striatal–cortical assembloids (Reumann et al., 2023). More recently, in 2025, a model of the ascending neural sensory pathway was established by connecting organoids representing the somatosensory system, spinal cord, thalamus, and cortex (Kim et al., 2025).

As a functional application of brain organoids, their potential use in bio-computing systems has attracted growing interest. In 2022, the concept of "Organoid Intelligence" was proposed as an emerging interdisciplinary field that aims to harness the self-organizing capabilities of brain organoids to perform learning and memory functions within bio-computing platforms (Smirnova et al., 2023).

To achieve these goals, it is essential to establish detailed methods for evaluating the electrical activity of brain organoids. Currently, electrophysiological functional assessments of organoids employ techniques such as patch-clamp recordings, calcium imaging, and microelectrode array (MEA) recordings. MEA-based approaches allow for long-term, non-invasive monitoring of the electrical activity of brain organoids and assembloids, enabling the observation of time-dependent changes in network dynamics and the evaluation of pharmacological responses (Tasnim and Liu, 2022; Lv et al., 2023; Pan et al., 2024). Moreover, analysis of low-frequency signals (below 500 Hz) has been shown to be effective for assessing pharmacological responses in brain organoids (Yokoi et al., 2021). In addition, disease-specific frequency characteristics and responses to contraindicated compounds have also been successfully detected (Yokoi et al., 2023). Recently, the development of high-density (HD) CMOS-based MEAs utilizing complementary metal-oxide semiconductor (CMOS) technology has further improved the precision of neuronal network activity evaluation. Recordings from brain organoids using HD CMOS MEAs have enabled the quantification of dynamic single-cell firing rates and the calculation of propagation velocities (Schröter et al., 2022; Sharf et al., 2022). However, these evaluations have generally been limited to small recording areas and a restricted number of electrodes, falling short of capturing activity across the entire organoid.

In this study, we present an analytical approach for detailed evaluation of electrical activity in brain organoids using field potential imaging (FPI) with an ultra-high-density (UHD) CMOS microelectrode array (MEA) comprising 236,880 microelectrodes (10.52 μm × 10.52 μm) across a wide sensing area of 32.45 mm^2 (Suzuki et al., 2023). Building on the basic recording capabilities demonstrated in previous work by Suzuki et al. (2023), this approach enables single-cell spike identification and detailed analysis of neuronal network connectivity. Additionally, we introduce propagation velocity and propagation area as new endpoints for network activity, which were previously unattainable with conventional MEAs due to their limited electrode density. Furthermore, we performed spatial analysis of frequency-specific signal characteristics across the organoids, revealing insights into the spatial distribution of different frequency bands. We also applied the UHD-CMOS MEA to midbrain–striatal assembloids to record electrical activity from both tissues and analyze inter-regional connectivity. This high-resolution methodology provides new insights into the functional dynamics of brain organoids and assembloids that were not achievable with traditional techniques.

2 Materials and methods

2.1 Culture of human iPS cells

Human induced pluripotent stem cells (hiPSCs) derived from a healthy donor (201B7 line, obtained from RIKEN) were cultured in 6-well plates pre-coated with Vitronectin (07180, STEMCELL Technologies) using mTeSR™ Plus medium (100-0276, STEMCELL Technologies). The culture medium was partially replaced (50%) every 3–4 days. Once the cells reached confluence, they were dissociated using Gentle Cell Dissociation Reagent (07174, STEMCELL Technologies) and subsequently used for organoid generation.

2.2 Culture of midbrain organoids

Midbrain organoids used in this study were pre-generated and supplied by STEMCELL Technologies. After acquisition, the organoids were cultured for four months using the STEMdiff™ Neural Organoid Maintenance Kit (100-0120,

STEMCELL Technologies). The culture medium was then replaced with BrainPhys™ Neuronal Medium (05792, STEMCELL Technologies), and complete medium changes were carried out every 3–4 days to maintain the organoids.

2.3 Culture of cerebral organoids

Cortical organoids were generated using the STEMdiff™ Cerebral Organoid Kit (08570, STEMCELL Technologies). Human iPS cells were seeded at a density of 9.0×10^3 cells per well, using EB seeding medium. On days 2 and 4 of culture, 100 μL of EB formation medium was added to each well. On day 5, the medium was replaced with induction medium, and the cultures were incubated for 2 days. On day 7, organoids were embedded in Matrigel (354277, Corning) and incubated in expansion medium for 3 days. From day 10 onward, the expansion medium was replaced with maturation medium, and the organoids were cultured on an orbital shaker (COSH6, AS ONE Corporation). Organoids were maintained in maturation medium for 3 months, with medium changes carried out every 3–4 days. After 3 months, the culture medium was switched to BrainPhys™ Neuronal Medium (05792, STEMCELL Technologies) for long-term maintenance. Details of the media components and kit reagents are provided in Supplementary Table 1.

2.4 Culture of midbrain–striatal assembloids

Midbrain–striatal assembloids were generated using the STEMdiff™ Midbrain Organoid Differentiation Kit (100-1096, STEMCELL Technologies) and the STEMdiff™ Dorsal Forebrain Organoid Differentiation Kit (08620, STEMCELL Technologies). To induce striatal differentiation, organoids were cultured in medium supplemented with Activin A, IWP-2, and SR11237, following the manufacturer's recommended conditions. Human iPSCs were seeded at a density of 3×10^6 cells per well in Organoid Formation Medium supplemented with 10 μM Y-27632, using AggreWell™800 24-well plates (34811, STEMCELL Technologies) pretreated with AggreWell Rinsing Solution (07010, STEMCELL Technologies). From days 2 to 5, half-medium changes were performed. On day 6, the culture medium was replaced with Midbrain Organoid Expansion Medium for midbrain organoids and Striatal Organoid Expansion Medium for striatal organoids. Full medium changes were performed every other day until day 25. On day 25, the respective Organoid Differentiation Media were introduced, and the same schedule of complete medium changes continued until day 43. From day 43 onward, cultures were maintained in Organoid Maintenance Medium. On day 50 (midbrain) and day 60 (striatal), one organoid of each type was placed together in a well of a 24-well plate and co-cultured on an orbital shaker (COSH6, AS ONE Corporation) to form midbrain–striatal assembloids. These assembloids were maintained in Maintenance Medium for an additional 4 months, with medium changes every 3–4 days. Details of the media components and kit reagents are provided in Supplementary Table 2.

2.5 Immunocytochemistry

Cultured brain organoids were fixed in 4% paraformaldehyde (PFA) in phosphate-buffered saline (PBS). After fixation, the organoids were embedded in Optimal Cutting Temperature (OCT) compound (45833, Sakura Finetek Japan), and 10 μm-thick cryosections were prepared using a cryostat (CM1950, Leica). The sections were first permeabilized with 0.2% Triton X-100 for 10 min and then incubated in pre-blocking buffer (PBS containing 0.05% Triton X-100 and 5% goat serum) at 4°C for 60 min. Primary antibody incubation was carried out in pre-blocking buffer at 4°C for 12 h using anti-MAP2 antibody (ab5392, Abcam) and anti-tyrosine hydroxylase (TH) antibody (ab137869, Abcam). For fluorescence detection, Alexa Fluor 488-conjugated anti-rabbit IgG (A11040, Invitrogen) and Alexa Fluor 546-conjugated anti-chicken IgG (A11008, Invitrogen) were diluted 1:1000 in pre-blocking buffer and incubated at room temperature for 1 h. Nuclear staining was performed with 1 μg/mL Hoechst 33258 (343-07961, Dojindo) for 1 h at room temperature. Fluorescently labeled organoid sections were imaged using a confocal laser scanning microscope (AX R, Nikon), and image analysis was performed using ImageJ software (NIH).

2.6 Ultra-high-density CMOS MEA recording

We employed a field potential imaging (FPI) method based on an ultra-high-density CMOS microelectrode array (UHD-CMOS MEA, Sony Semiconductor Solutions) to measure the electrical activity of brain organoids. The MEA comprises 236,880 platinum electrodes (10.52 μm × 10.52 μm; 110.67 μm^2 each), providing a total recording area of 32.45 mm^2. The device features a three-layer stacked chip architecture in which an analog chip for signal acquisition is connected to two digital logic chips for signal processing via 38,000 micro-bumps. Integrated single-slope analog-to-digital converters (SS-ADCs) enable 33,840 readout channels to operate at 70 kSamples/s, thereby allowing data acquisition from all 236,880 electrodes at an effective sampling rate of 10 kSamples/s (Kato et al., 2020). Cerebral organoids, midbrain organoids, and midbrain–striatal assembloids were carefully placed onto the electrode surface within the recording well of the UHD-CMOS MEA system. After positioning, the culture medium was gently aspirated to bring the organoid into close contact with the electrode surface. Subsequently, a small volume of fresh culture medium was slowly added to the well to prevent the organoid from floating, while preserving tissue integrity. This procedure allowed stable adherence of the organoid to the electrode surface without causing mechanical damage. Recordings were conducted under controlled environmental conditions (5% CO_2, 37°C). Electrical signals were acquired at sampling rates of either 2 kHz or 10 kHz, depending on the experimental design. Specifically, recordings of midbrain organoids were performed at 10 kHz, whereas those of cerebral organoids and midbrain–striatal assembloids were conducted at 2 kHz. To stabilize the baseline, signal drift was removed using least-squares

detrending applied to each 500-sample segment, followed by offset correction.

2.7 Pharmacological assays

Pharmacological experiments were conducted to evaluate the responsiveness of brain organoids to neurotransmitter-related agents. In 4-months-old midbrain organoids, 3-(3,4-dihydroxyphenyl)-L-alanine (L-DOPA; D0600, Tokyo Chemical Industry), a dopamine precursor, was applied to three organoids ($n = 3$), and spontaneous electrical activity was recorded for 2 min at each concentration. In 5-months-old cerebral organoids, the $GABA_A$ receptor antagonist picrotoxin (PTX; 168-17961, FUJIFILM Wako) and the NMDA receptor antagonist MK-801 (M107-50MG, Sigma) were each applied to three separate organoids ($n = 3$ for each condition), and spontaneous activity was recorded for 1 min at each concentration. Additionally, to assess changes in inter-regional connectivity within midbrain–striatal assembloids, 4-aminopyridine (4-AP; 016-02781, FUJIFILM Wako) was applied to a 4-months-old assembloid ($n = 1$), and spontaneous activity was recorded for 2 min at each concentration. All compounds were applied sequentially to the same organoid using a cumulative dosing protocol. After each application, the organoid was incubated for 5 min before recording.

2.8 Spike detection and soma identification

Spike detection was performed on voltage signals processed with a 100 Hz high-pass filter, using a threshold of $\pm 5.0\sigma$, where σ denotes the standard deviation of baseline noise during a quiescent period. Events exceeding this threshold were defined as spikes. For each detected spike, a waveform segment comprising 20 samples before and after the spike time point (41 samples in total) was extracted. Waveforms with a standard deviation below 13 were considered noise and excluded from further analysis. Soma identification was then performed based on spike timing correlations between electrode pairs. For all electrode pairs in which spikes were detected, inter-spike intervals (ISIs) were calculated. If the ISI between spikes on two electrodes was less than 10 ms, it was counted as a same-count event. Electrode pairs with ≥ 5 same-counts that also constituted $\geq 15\%$ of all possible spike pairs were designated as putative somatic electrode pairs. If the distance between electrodes in a putative pair was less than 50 μm, they were considered to originate from the same neuronal soma, and the location was identified as a somatic candidate site. In the case of midbrain organoids, spike events occurring during network bursts were excluded from soma identification to minimize false positives. All data analysis, including signal filtering, spike detection, frequency decomposition, and network analysis, was performed using MATLAB scripts and custom software on a workstation running Windows 11 Pro. The system was equipped with an Intel® Core™ i9-14900K CPU (3.20 GHz), 128 GB of RAM, an NVIDIA GeForce RTX 4080 SUPER GPU, and more than 6 TB of SSD storage. This computational environment was used consistently across all analysis procedures described in Sections "2.8 Spike detection and soma identification" through "2.12 Analysis of connection strength in midbrain–striatal assembloids."

2.9 Z-score analysis

Z-score Analysis was performed using custom MATLAB scripts. For each neuronal pair, a synchronous spike was defined as an event in which a spike from one cell was followed by a spike from the other cell within 100 ms. The total number of synchronous spikes was counted for each pair. To assess statistical significance, 100 surrogate spike trains were generated by randomly shuffling the original spike time sequences while preserving each cell's inter-spike interval (ISI) distribution. For each surrogate dataset, the number of synchronous spikes was calculated using the same criteria. A z-score was calculated using the mean and standard deviation of the synchronous spike counts across the surrogate datasets, based on the synchronous spike count in the actual data. A z-score ≥ 3 was considered to indicate significant spike synchrony between the two cells, and such pairs were defined as having a functional connection. Based on the results of the z-score analysis, the number of significantly connected partner cells was counted for each neuron to determine its connection degree.

2.10 Propagation analysis

Propagation analysis was implemented in MATLAB using custom scripts. Oscillatory activity was detected in voltage waveforms recorded using the UHD-CMOS MEA. Electrodes that exhibited signal amplitudes ≥ 30 μV during these periods were defined as propagating electrodes, while all others were treated as noise electrodes and excluded from the analysis. For each propagating electrode, the peak time–defined as the interval from the onset of oscillation ($t = 0$) to the point of maximum amplitude–was calculated. A time-series dataset was then constructed by counting the number of electrodes that reached their peak within each time bin. The propagation velocity of network activity was estimated by computing the temporal derivative of this time series. Velocity measurements were obtained for each oscillatory event at each drug concentration and were subsequently averaged within individual organoids to yield a single mean value per concentration per organoid. These organoid-level means were then used for group-level comparisons across concentration groups.

2.11 Frequency band power analysis of oscillatory waveforms

Frequency band power analysis was performed using MATLAB. Detected oscillatory waveforms were processed using zero-phase filtering with a finite impulse response (FIR) bandpass filter to isolate signals within distinct frequency bands. The potential amplitude for each frequency band was calculated from the filtered waveforms. The five frequency bands analyzed were defined as follows: delta (0.5–3 Hz), theta (4–7 Hz), alpha (8–11 Hz), beta (12–29 Hz), and gamma (30–100 Hz). For each band, power values were standardized using the mean and standard

deviation across all electrodes. The resulting normalized data were subjected to unsupervised clustering using the k-means algorithm implemented in MATLAB (MathWorks) to classify patterns of frequency-specific potential dynamics.

2.12 Analysis of connection strength in midbrain–striatal assembloids

Connection strength analysis was conducted using MATLAB. For each neuronal pair, a synchronous spike was defined as a spike from one cell followed by a spike from the other cell within 100 ms. The number of synchronous spikes was counted for each pair. To minimize the influence of differences in firing rates between cells, the synchronous spike count was normalized by the mean spike count of the respective cell pair. The resulting value was defined as the connection strength. Connection strength was calculated separately for three groups: striatal organoids, midbrain organoids, and midbrain–striatal assembloids.

2.13 Statistical analysis

All statistical analyses were performed using one-way analysis of variance (ANOVA), followed by Dunnett's *post-hoc* test for multiple comparisons. For pharmacological assays, comparisons were made between the baseline (pre-treatment) condition and each drug concentration group. A p-value of less than 0.05 was considered statistically significant. In addition to significance testing, effect size analyses were performed to evaluate the magnitude of drug-induced changes. Eta squared (η^2) was calculated to assess the overall treatment effect across all concentrations relative to baseline. For pairwise comparisons between the baseline and each drug concentration, Cohen's d was computed. All results are presented as group means ± standard error of the mean (SEM). Detailed statistical outcomes, including p-values and effect size estimates for all comparisons, are provided in Supplementary Table 3.

3 Results

3.1 Single-cell firing rate and intercellular connectivity analysis of midbrain organoids following L-DOPA administration

Immunofluorescence staining of midbrain organoids derived from human iPSCs and cultured for 4 months confirmed the expression of MAP2, a marker for mature neurons, and TH, a marker for dopaminergic neurons (Figure 1A). In addition, non-TH-positive neurons were present. The midbrain organoid was mounted on a UHD-CMOS MEA (Figure 1B), and spontaneous electrical activity was recorded across the entire organoid, resulting in the identification of 404 individual cells. A raster plot and histogram of the spontaneous spike activity over a 2-min period from these identified cells are shown in Figure 1C. Network bursts, in which almost all cells spiked simultaneously, were observed (indicated by peaks in the histogram and vertical black lines in the raster plot in Figure 1C), suggesting the formation of functional neuronal circuits within the midbrain organoid. Cumulative administration of the dopamine precursor L-DOPA to three midbrain organoids resulted in a dose-dependent increase in total spike count, reaching 122.3% ± 25.1 at 0.3 μM, 127.6% ± 16.8 at 3 μM, and 148.0% ± 25.3 at 30 μM, relative to the baseline (Figure 1D). Notable increases in total spike count were observed at 30 μM (p = 0.0158, Cohen's d = 5.4641), supporting the interpretation that L-DOPA administration elicited a physiologically meaningful response in midbrain organoids. To investigate the cellular and network-level responses to L-DOPA in greater detail, one of the three midbrain organoids was selected for in-depth analysis. Figure 1E presents a spatial map of total spike counts over 2 min for the 404 identified cells, with dot size representing the number of spikes. Cells whose spike count increased to ≥150% following administration of L-DOPA (30 μM) compared to before treatment are shown in red, while those with a decrease to ≤50% are shown in blue. The proportion of cells with increased activity was 19.3% at 0.3 μM, 39.4% at 3 μM, and 59.7% at 30 μM. Conversely, the proportion of cells with decreased activity was 10.1%, 2.23%, and 0.495%, respectively, while the proportions of non-responsive cells were 70.5%, 58.4%, and 39.9%, respectively (Figure 1F). The single-cell resolution afforded by the UHD-CMOS MEA enabled the detection not only of increased spike activity following L-DOPA treatment but also of cells that were non-responsive or showed suppressed activity at lower doses. To evaluate network activity in the midbrain organoid, z-scores were calculated for cell pairs that spiked within 100 ms. In Figure 2A, black lines indicate cell pairs with a z-score ≥ 3 before L-DOPA administration, while blue lines indicate pairs whose z-scores increased after treatment. L-DOPA administration led to a dose-dependent increase in connection strength (Figure 2B). The distribution of z-scores also shifted to the right in accordance with L-DOPA concentration (Figure 2C), suggesting enhanced synchrony within the network. To quantitatively assess changes in connection strength, cell pairs with z-scores ≥ 3 were defined as connected, and the average number of connected cells per cell was calculated. The number of connections per cell, calculated from 404 identified cells, was 333.2 ± 84.6 at baseline, 335.8 ± 79.2 at 0.3 μM, 380.5 ± 42.8 at 3 μM, and 382.7 ± 45.2 at 30 μM (n = 404 cells; Figure 2D). Notable increases were observed at 3 μM (p = 0.0001, Cohen's d = 0.63) and 30 μM (p = 0.0004, Cohen's d = 0.66), supporting the interpretation that L-DOPA enhanced network connectivity in a dose-dependent manner. These findings indicate that the UHD-CMOS MEA enables both single-cell spike analysis and intercellular connectivity evaluation in brain organoids.

3.2 Analysis of propagation velocity and propagation area in cortical organoids

The ultra-high-density (UHD) CMOS MEA, with its high temporal and spatial resolution, enabled the derivation of novel endpoints for evaluating network activity in brain organoids–specifically, propagation velocity and propagation

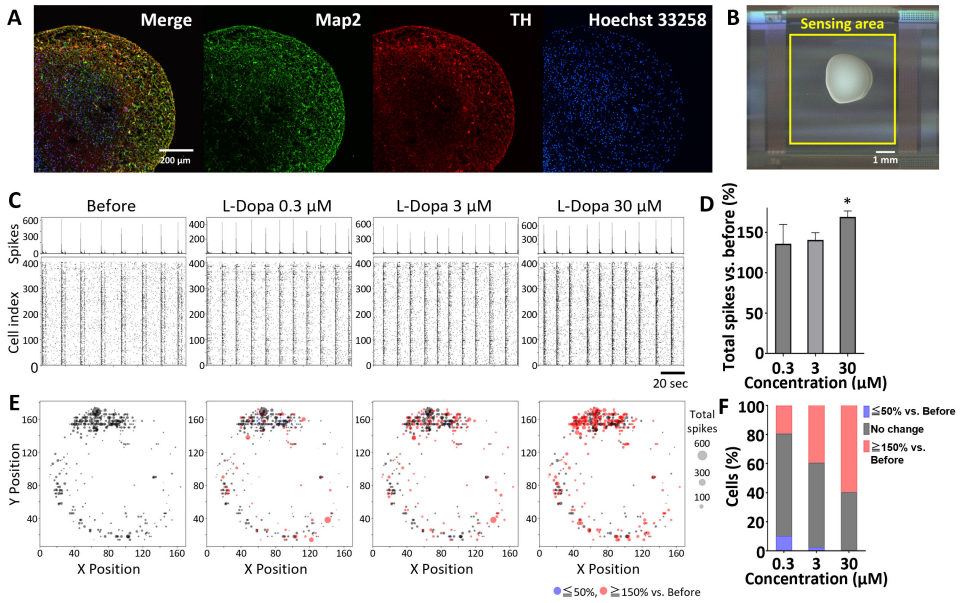

FIGURE 1
Single-cell spike analysis of midbrain organoids. **(A)** Immunofluorescence image of a human midbrain organoid cultured for 4 months. Green: MAP2; red: TH; blue: Hoechst 33258. Scale bar = 200 µm. **(B)** Midbrain organoid mounted on a UHD-CMOS MEA. The sensing area is indicated by a yellow square. Scale bar = 1 mm. **(C)** Raster plot and histogram of spontaneous neuronal spikes over a 2-minute period before and after L-DOPA administration. Scale bar = 20 s. **(D)** Total spikes recorded during a 2-min period before and after L-DOPA administration. For each concentration, values were normalized to the pre-treatment (before) level and averaged (n = 3 organoids). Error bars represent the standard error of the mean (SEM). Data were analyzed using one-way ANOVA followed by Dunnett's post hoc test (*p < 0.05 vs. before). **(E)** Spatial map of spontaneous spikes over a 2-minute period from 404 detected cells within a single organoid. Each dot represents a cell body, and dot size reflects spike frequency. Red: ≥ 150% vs. before; blue: ≤ 50% vs. before. **(F)** Change in spike frequency following L-DOPA administration in the same organoid. The proportion of cells showing altered activity relative to before administration is indicated. Red: ≥ 150% vs. before; blue: ≤ 50% vs. before; black: no change.

area. To assess propagation velocity, the GABA_A receptor antagonist picrotoxin (PTX) was applied to three 5-months-old cerebral organoids. Figure 3A shows representative propagation waveforms recorded during spontaneous oscillations, with the corresponding electrode positions indicated by red arrows in the top-left panel of Figure 3B (Before). Peak timing maps of oscillatory waveforms across electrodes, recorded before and after PTX administration, are presented in Figure 3B, illustrating that neural activity propagated throughout the entire organoid. Propagation velocity was calculated by differentiating the number of electrodes reaching peak voltage per unit time (Figure 3C). Compared to the baseline, propagation velocity significantly increased to 127.8% ± 5.13 at 0.1 µM (p = 0.00477, Cohen's d = 3.13), 120.0% ± 4.92 at 1 µM (p = 0.0279, Cohen's d = 2.35), and 128.1% ± 4.95 at 10 µM (p = 0.00482, Cohen's d = 3.27), respectively (Figure 3C). Propagation area was assessed before and after treatment with the NMDA receptor antagonist MK-801, using three cerebral organoids. In the maps shown in Figure 3D, electrodes exhibiting propagation activity are indicated in black. Compared to the baseline, propagation area showed a concentration-dependent reduction, reaching 97.1% ± 13.2 at 0.1 µM (p = 0.994, Cohen's d = −0.125), 59.6% ± 7.27 at 1 µM (p = 0.0501, Cohen's d = −3.21), and 40.8% ± 12.9 at 10 µM (p = 0.00713, Cohen's d = −2.65), respectively (Figure 3C). At 1 µM, although a marked reduction in propagation area was generally observed, localized increases were also apparent in certain organoids, such as in the lower right region shown in Figure 3D. These findings indicate that the analysis of propagation velocity and propagation area using UHD-CMOS MEAs provides an effective approach for evaluating compound-induced responses related to synaptic transmission in brain organoids.

3.3 Frequency characteristics of cerebral organoids

Field potential imaging (FPI) using the UHD-CMOS MEA provides voltage waveforms, making it suitable for frequency analysis in a manner analogous to conventional MEA recordings. Figure 4A displays a representative raw waveform recorded from a single electrode in a 5-months-old cerebral organoid, alongside corresponding signals filtered into delta (0.5–3 Hz), theta (4–7 Hz), alpha (8–11 Hz), beta (12–29 Hz), and gamma (30–100 Hz) bands using a finite impulse response (FIR) bandpass filter. When a network burst occurred across the entire cortical organoid, slow-wave field potentials were observed, as shown in Figure 4A. For frequency-domain analysis, field potentials were acquired from up to 46,630 electrodes across three cerebral organoids. Figure 4B shows heatmaps of standardized potential intensities for each frequency band across all electrodes. Across all three organoids (organoids 1–3), gamma-band activity exhibited a spatial distribution distinct from those observed in the delta to beta bands. For example, in organoid 1, a spatial gradient was observed in the delta

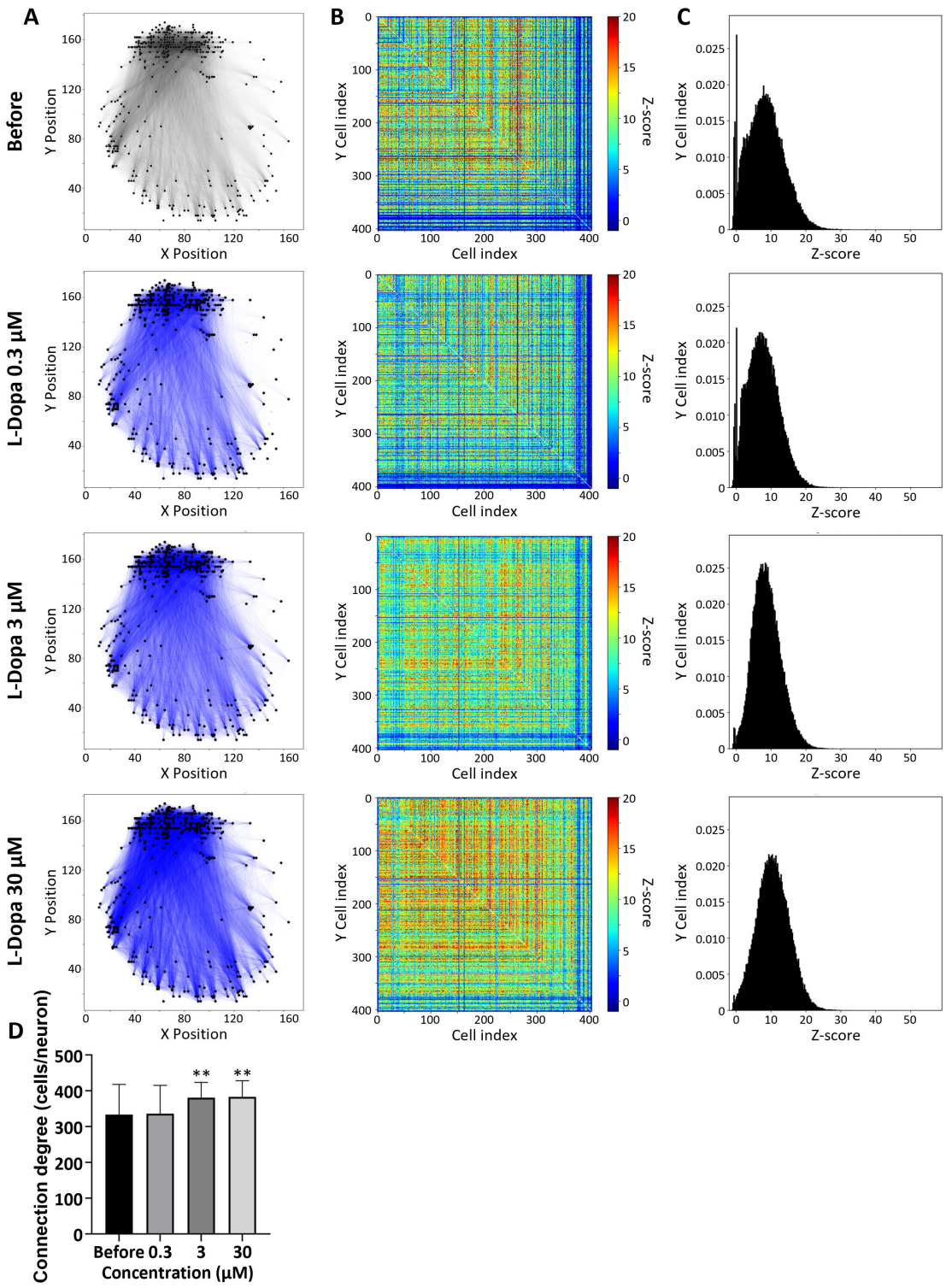

FIGURE 2
Neural network analysis of midbrain organoids. Changes in connection strength between cell pairs before and after L-DOPA administration. To evaluate network activity, z-scores were calculated for cell pairs that spiked within 100 ms. **(A)** Cell connection map. Black lines indicate cell pairs with a z-score = 3; blue lines indicate pairs whose z-score increased after L-DOPA treatment. **(B)** Heatmap of z-scores for 404 detected cells. **(C)** Distribution of z-scores. **(D)** Change in the number of connected cells per individual cell. Error bars represent the standard error of the mean (SEM). Data were analyzed using one-way ANOVA followed by post hoc Dunnett's test (**$p < 0.01$ vs. before).

to beta bands, with higher intensities generally radiating from the periphery toward the center, and the strongest signals consistently detected in the lower-right region. In contrast, gamma-band signals in this organoid were weaker in the lower half and stronger in the upper half, forming a spatial pattern that clearly diverged from that of the lower-frequency bands.

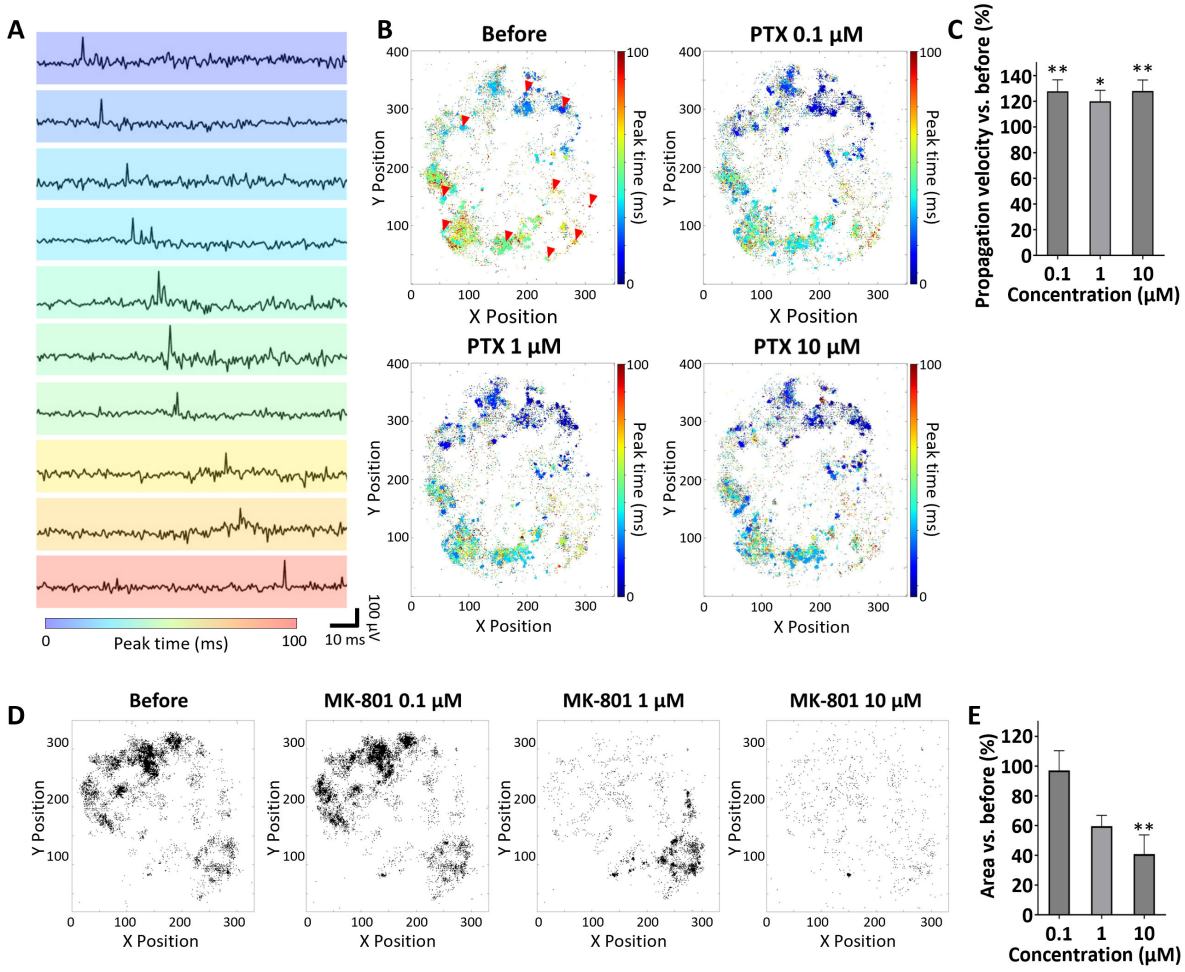

FIGURE 3
Propagation analysis of cortical organoids. **(A)** Spontaneous activity propagation waveform color-coded by the timing of voltage peaks. The electrode used for pickup is indicated by a red arrow in **(B)** Before. **(B)** Delay maps of oscillation peak timing before and after picrotoxin (PTX) administration. **(C)** Propagation velocity before and after PTX administration. Propagation velocity was calculated per oscillation event and averaged within each organoid at each concentration. Values from three organoids were used per concentration (n = 3 organoids per group). All drug concentrations were applied sequentially to the same organoids following a cumulative dosing protocol. Data were analyzed using one-way ANOVA followed by *post hoc* Dunnett's test (*p < 0.05, **p < 0.01 vs. before). **(D)** Electrode maps showing propagation before and after MK-801 administration; black dots indicate propagation electrodes. **(E)** Propagation area before and after MK-801 administration. Propagation area was calculated per oscillation event and averaged within each organoid at each concentration. Values from three organoids were used per concentration (n = 3 organoids per group). MK-801 was administered according to the same cumulative dosing protocol. Data were analyzed using one-way ANOVA followed by *post hoc* Dunnett's test (**p < 0.01 vs. before).

This difference highlights frequency-specific spatial organization within the brain organoid. To delineate spatial domains with distinct frequency characteristics, k-means clustering analysis was performed on data from one organoid in which 46,630 electrodes recorded usable signals. This analysis segmented the organoid into nine distinct spatial clusters (Figure 4C). Comparison of the frequency intensity profiles across clusters revealed that Clusters 1–3 exhibited low intensity across all bands, whereas Clusters 5, 7, and 8 showed uniformly high intensity. Clusters 6 and 9 exhibited high intensity in the delta to beta bands but relatively low gamma-band activity (Figure 4D). Frequency analysis of activity waveforms detected from 46,630 electrodes on the UHD-CMOS MEA demonstrated that region-specific frequency characteristics can be extracted from the brain organoid.

3.4 Inter-regional connection analysis in midbrain–striatal assembloids

Using the UHD-CMOS MEA, we recorded the electrical activity of midbrain–striatal assembloids and evaluated inter-regional connection strength based on single-cell firing activity. Figure 5A shows a heatmap of peak voltage distribution over a 1-min recording period, where the upper part corresponds to the striatum and the lower part to the midbrain organoid. Electrical activity was detected in both regions, indicating that each tissue was functionally active. To assess the effects of pharmacological intervention, 30 µM of 4-aminopyridine (4-AP), a potassium channel blocker, was administered to the assembloid, and changes in firing frequency and inter-regional connectivity were evaluated. Figure 5B presents raster plots of individual cells (red: striatum,

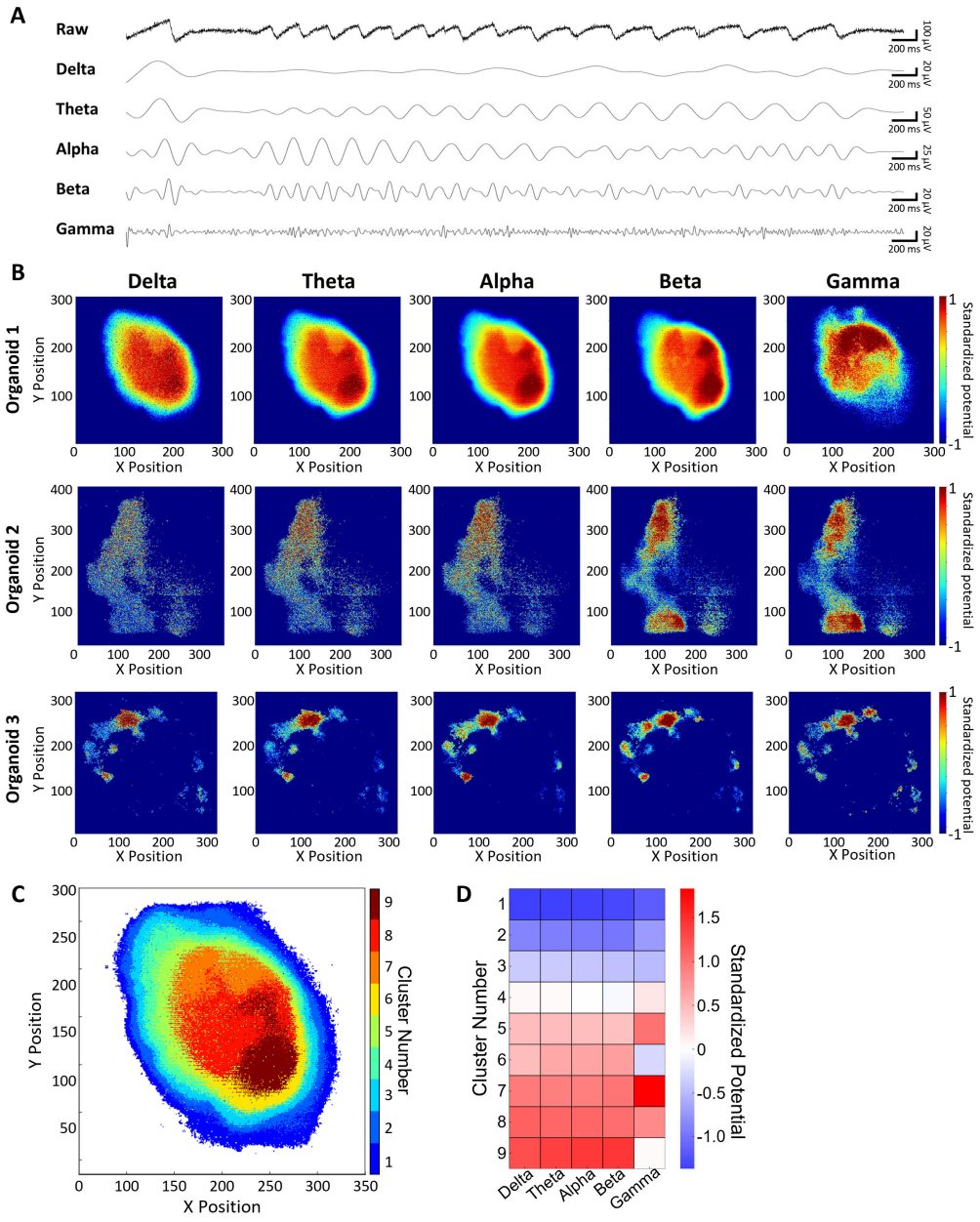

FIGURE 4
Frequency distribution characteristics of cortical organoids. **(A)** Spontaneous oscillation waveforms for each frequency band. From top to bottom: raw waveform, delta, theta, alpha, beta, gamma. **(B)** Spatial distribution maps of normalized signal intensity for each frequency band, presented for three independent cerebral organoids (one per row). Each column represents a different frequency band (from left to right: delta to gamma), enabling comparison of spatial patterns across organoids. **(C)** Clustering map showing nine groups classified based on the intensity profiles of five frequency bands. **(D)** Heatmap of frequency band intensities for each cluster.

yellow: midbrain). Following 4-AP administration, spike counts increased in both the midbrain and striatum (Figure 5C). Connection strength was calculated by normalizing the number of synchronized spikes (defined as spikes occurring within 100 ms between neuron pairs) by the average firing rate of each pair. Figure 5D shows the connection strength within the striatum, within the midbrain, and between the midbrain and striatum before and after 4-AP treatment. The connection strength increased from 0.0360 to 0.0946 within the striatum and from 0.181 to 0.377 within the midbrain. Furthermore, the inter-regional connection strength between the midbrain and striatum also increased from 0.0305 to 0.0632. Single-cell-based network connectivity analysis using the UHD-CMOS MEA revealed that changes in inter-organoid information transmission within assembloids can be detected following compound administration.

4 Discussion

In this study, we performed large-scale recordings of brain organoids using field potential imaging (FPI) with an ultra-high-density (UHD) CMOS microelectrode array (MEA) comprising

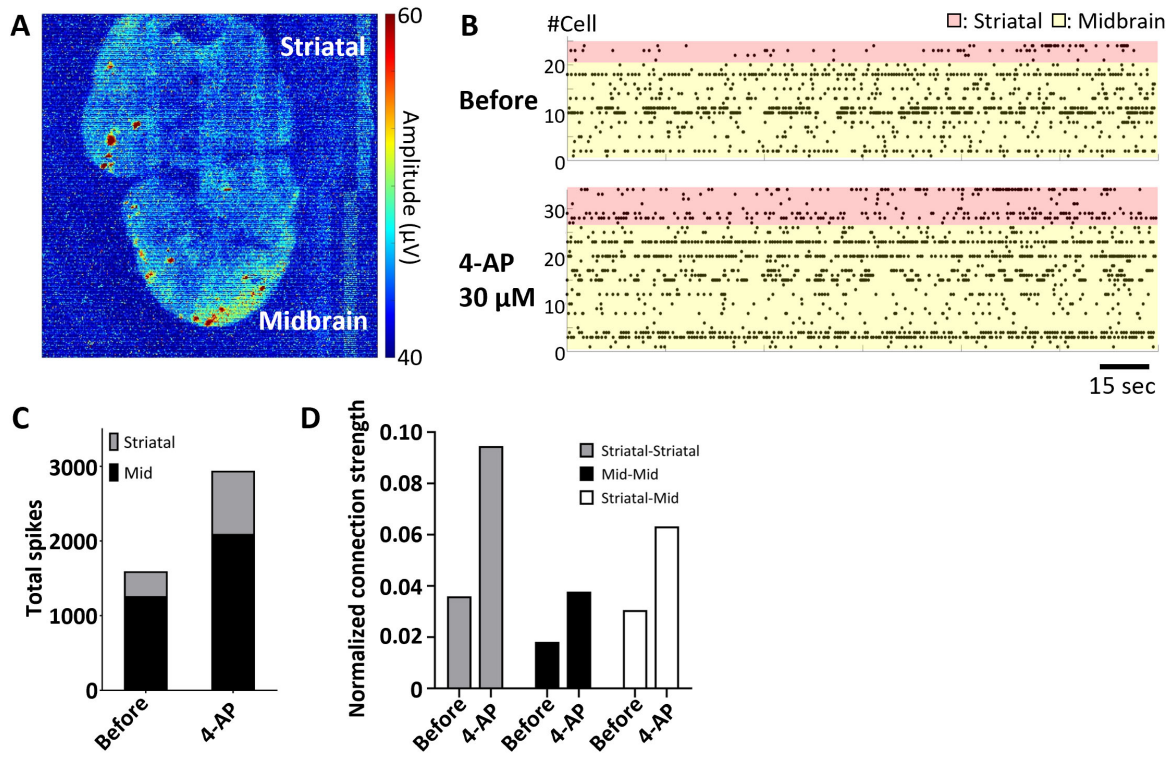

FIGURE 5
Analysis of inter-regional connectivity in midbrain–striatal assembloids. **(A)** Peak potential map of spontaneous activity over a 1-min recording. Upper region: striatum; lower region: midbrain. **(B)** Raster plot of spontaneous spikes from individual cells over 1 min. Red: striatum; yellow: midbrain. Scale bar = 15 s. **(C)** Total spike count before and after 4-AP administration. The total number of spikes per minute is shown for each region. Gray: striatum; black: midbrain. **(D)** Connection strength before and after 4-AP administration. Strength was calculated by normalizing the number of synchronous spikes (within 100 ms) by the mean spike count of each cell pair. Gray: within striatum; black: within midbrain; white: between midbrain and striatum. Data shown in this figure were obtained from a single midbrain–striatal assembloid (n = 1).

236,880 microelectrodes (each measuring 10.52 μm × 10.52 μm) and covering a broad sensing area of 32.45 mm^2, in order to precisely characterize the detailed electrical activity of brain organoids. Based on single-cell activity, we analyzed neuronal network connectivity, propagation velocity, propagation area, and frequency characteristics.

L-Dopa, a precursor to dopamine, is taken up by neurons and decarboxylated by Aromatic L-Amino Acid Decarboxylase (AADC), resulting in the production of dopamine, which is subsequently released into the extracellular space. When L-Dopa was administered to midbrain organoids, a decrease in activity was observed in 10.1% of cells at a concentration of 0.3 μM (Figure 1F). TH-positive dopaminergic neurons are known to express D2 autoreceptors (Beaulieu and Gainetdinov, 2011), and this suppression of activity is thought to be due to D2 receptor activation following dopamine release. However, at higher concentrations, this suppression was no longer observed (Figure 1E), and instead, an enhancement of network activity was seen throughout the midbrain organoids (Figure 2A). The midbrain organoids used in this study contained not only TH-positive neurons (Figure 1A) but also likely included vglut2-positive glutamatergic neurons, which are known to be present in the midbrain, as well as cells expressing D1-type dopamine receptors (Yamaguchi et al., 2007; Yamaguchi et al., 2011; Morales and Root, 2014). It is possible that excitatory input from these cells indirectly disinhibited or activated dopaminergic neurons, leading to increased activity at the single-cell level (Figure 1E) and strengthened network connectivity across the entire organoid (Figure 2A). Importantly, the combination of single-cell spike detection and large-scale connectivity profiling uniquely enabled by the UHD-CMOS MEA platform allowed us to resolve cell-type–specific and spatially heterogeneous responses to L-DOPA–features that would likely remain undetectable using conventional MEAs or bulk recording techniques. This analysis, based on a single representative midbrain organoid, highlights the ability of the UHD-CMOS MEA platform to capture dynamic, circuit-level changes induced by pharmacological interventions.

Based on the capabilities of the UHD-CMOS-MEA, novel endpoints for the propagation velocity and area of network activity were established. In cortical organoids, the propagation velocity of network activity increased following administration of picrotoxin (PTX), a $GABA_A$ receptor antagonist. This observation aligns with previous reports showing that administration of bicuculline methiodide–another $GABA_A$ receptor antagonist–increased propagation velocity in cortical slices derived from human epilepsy patients (Covelo et al., 2025). Although the compounds differ, the results may reflect similar physiological effects mediated by $GABA_A$ receptor inhibition. Following administration of MK-801, an NMDA receptor antagonist, a reduction in the propagation area was observed in most regions of the organoids (Figures 3D, E). Similar reductions in activity propagation caused by NMDA receptor antagonists have been

reported in *in vivo* EEG recordings from rats and in brain slice experiments (Morales-Villagrán et al., 1996; Fukuda et al., 1998), suggesting that the responses observed in this study may reflect physiological phenomena in the intact brain. Notably, while the propagation area decreased across most regions of the organoid, localized enhancements in propagation were observed in some organoids–for example, in the lower-right region of the sample shown in Figure 3D following treatment with 1 μM MK-801. This focal increase in activity may be attributable to disinhibition resulting from impaired function of GABAergic neurons. Previous studies have described both direct suppression of inhibitory neuron activity via NMDA receptor blockade and indirect effects through reduced excitatory input (Li et al., 2002; Homayoun and Moghaddam, 2007). These mechanisms are considered to underlie the excitotoxic effects of NMDA receptor antagonists. Due to self-organization, brain organoids likely exhibit regional variability in the ratio of excitatory to inhibitory neurons. Consequently, in areas with a lower proportion of inhibitory neurons, the loss of inhibitory control induced by MK-801 may be more pronounced, potentially leading to enhanced excitatory activity mediated by AMPA receptors. Analysis of propagation velocity and propagation area using the UHD-CMOS MEA demonstrated that this method is effective for evaluating compound responses related to synaptic transmission in brain organoids. Moving forward, integrating analyses of propagation pathways may enable the identification of regions exhibiting disease-related activity abnormalities or neural circuits serving as initiation sites for compound responses.

Since FPI represents voltage waveforms, frequency analysis can be conducted similarly to conventional MEA measurements. Traditional frequency analyses of brain organoids using standard MEAs were limited by the small number of electrodes, typically ranging from 16 to 64. In this study, activity was acquired from up to 46,630 electrodes using the UHD CMOS MEA, which enabled a comprehensive analysis of frequency distributions across the entire organoid. In organoid1, delta band potentials increased from the periphery toward the center. Alpha to beta band activity also intensified toward the center, with particularly strong signals observed in the lower-right region of the organoid. In contrast, gamma band activity displayed a distinct pattern–being stronger in the upper region and weaker in the lower region (Figure 4B, organoid1). To our knowledge, this is the first report to describe frequency-specific spatial architecture in brain organoids, particularly the differential distribution of gamma-band activity relative to lower frequency bands. Similar spatial features of gamma band activity were also observed in two additional cerebral organoids (organoid2 and organoid3), indicating that this frequency-specific pattern was consistently detected across samples (Figure 4B). Clustering analysis enabled visualization of the organoid's structural features based on frequency-specific characteristics (Figure 4C). However, because the organoids were measured without being anchored to the electrodes, the variability in adhesion between the organoid and electrodes must be considered. The periphery of the organoid likely had fewer cells adhering to the electrodes, which may explain the consistently weak potentials observed in clusters 1, 2, and 3 across all frequency bands. In contrast, clusters 6, 7, 8, and 9, located deeper within the organoid, exhibited variations in gamma band potentials (Figure 4C), indicating that in regions with better electrode contact, the intrinsic structural frequency properties of the organoid were more accurately reflected. The distribution of gamma band activity may be associated with the expression of PV-positive GABAergic neurons (Cardin et al., 2009), which are known to be essential for gamma wave generation in the cortex. In clusters 6 and 9, where gamma activity was weak while other frequency bands were strong, it is likely that PV-positive GABAergic neurons were either absent or functionally immature. Previous studies have shown that the expression of GABAergic neurons in cortical organoids increases after 6 months of culture (Trujillo et al., 2019). Given that the organoids in this study were 5 months old, it is plausible that some regions lacked sufficient expression or functional maturity of PV-positive GABAergic neurons. Although clustering was performed only for organoid1, the consistent gamma band distribution patterns observed in organoid2 and organoid3 support the generalizability of this spatial frequency profile across cortical organoid samples. Comparing the electrophysiological frequency characteristics of organoids with cell type identity and the histochemically organized circuit architecture within the organoids remains an important challenge for future studies. Taken together, these findings highlight both the strengths and limitations of the UHD CMOS MEA approach for frequency analysis in brain organoids. While technical factors such as variability in tissue-electrode contact and biological factors such as neuronal maturity must be taken into account, the high spatial resolution and wide coverage of this platform enable a detailed and spatially resolved assessment of frequency dynamics. This capability is particularly valuable for evaluating neurological disorders such as epilepsy, Alzheimer's disease, and autism, where gamma band activity plays a critical role (Herrmann and Demiralp, 2005; Başar, 2013; McNally and McCarley, 2016; Guan et al., 2022).

Currently, the evaluation of assembloids is primarily performed using techniques such as optogenetic observation with adeno-associated viruses (AAV), calcium imaging, patch-clamp recordings, and conventional multi-electrode arrays (MEAs) (Andersen et al., 2020; Miura et al., 2020; Reumann et al., 2023; Ozgun et al., 2024). However, these methods have limitations in terms of temporal and spatial resolution, as well as invasiveness to the cells. In contrast, the UHD CMOS MEA enabled the non-invasive detection of electrical activity at single-cell resolution across the entire assembloid, with both high temporal and spatial precision (Figure 5A). When 4-Aminopyridine (4-AP), a potassium channel blocker, was applied to midbrain–striatal assembloids, increased firing activity was observed in both the midbrain and striatal regions (Figure 5B). Furthermore, an enhancement of inter-regional connectivity was also detected (Figure 5C). Notably, the ability to capture coordinated activity across anatomically distinct regions–without the need for exogenous probes or genetically encoded indicators–highlights a unique advantage of the UHD CMOS MEA platform in studying functional integration within complex three-dimensional neural systems. A current limitation of this experimental setup is the inability to selectively apply compounds to individual tissues, leading to simultaneous exposure of both regions. This complicates the mechanistic analysis of inter-regional connection enhancement. One potential solution is to combine UHD CMOS MEA recordings with optogenetic techniques, such as AAV-mediated gene delivery, enabling targeted stimulation of specific cell types and subsequent recording of their responses. Additionally, integrating UHD CMOS MEA with Microphysiological System (MPS) devices containing

microfluidic channels would allow for region-specific compound administration. MPS platforms seed organoids into individual chambers connected via microfluidic pathways, offering both structural control and the ability to measure not only tissue-specific activity but also axonal signals transmitted through the connecting channels. A system that combines these technologies with UHD CMOS MEA for assessing inter-organ connectivity in assembloids may be particularly valuable for investigating projection deficits caused by neurological disorders. It may also be applied to disease models involving peripheral nervous system damage, such as those using sensory neuron–spinal cord assembloids.

Ultra-high-density CMOS microelectrode arrays technology offers high spatial and temporal resolution, enabling the simultaneous acquisition of electrical activity from over 46,000 electrodes in brain organoids. However, several limitations must be acknowledged. A fundamental constraint of extracellular recording is its inherent bias toward neurons located in close proximity to the electrode surface. In three-dimensional structures such as cerebral organoids or assembloids, neurons situated deeper within the tissue or on the surface opposite the electrodes may produce attenuated signals or fall below the detection threshold due to reduced signal-to-noise ratios. This spatial sampling bias can lead to overrepresentation of superficial neuronal activity and may distort network-level analyses such as burst detection, synchrony, and functional connectivity. Moreover, among the organoid samples examined, only a small subset exhibited global oscillatory activity across the entire tissue, whereas most showed only localized oscillations or no detectable electrical activity. Notably, even organoids derived from the same iPSC line and cultured under identical conditions frequently displayed substantial variability in electrophysiological activity. This variability is attributed primarily to intrinsic heterogeneity associated with the self-organizing nature of organoid development, which can result in differences in cellular composition and network maturation, even under standardized protocols. Although no summary data or representative examples were presented in the current work, this phenomenon was consistently observed across multiple independent batches and is considered a relevant methodological limitation. Elucidating the developmental stages or microenvironmental factors that contribute to such variability, and establishing criteria for identifying functionally mature organoids, remains an important goal for future research. While methods such as slicing or physical anchoring could potentially improve tissue–electrode contact, these approaches are often incompatible with the delicate architecture of intact 3D tissues and may compromise tissue viability or recording stability. Future strategies may involve the development of volumetric electrode arrays, integration with optogenetic tools, the use of microfluidic systems that allow spatially controlled stimulation and recording, or the design of physical anchoring systems optimized for organoids to improve electrode–tissue contact without compromising structural integrity. These technologies hold promise for enabling more comprehensive and reproducible functional recordings throughout the full volume of organoid models.

In this study, we established a methodology for large-scale recording of brain organoids using UHD-CMOS MEA, along with analytical techniques to assess network connectivity, propagation velocity, propagation area, and frequency dynamics at the single-cell level. The parameters based on spatial information, such as propagation velocity and propagation area, can now be measured with this system, which covers a wide area of 32.45 mm^2–an area that conventional CMOS MEAs cannot achieve. Additionally, the large-scale recording capacity (over 46,000 electrodes) allows for frequency-domain analysis at single-electrode resolution across the entire organoid, revealing region-specific frequency patterns. Notably, gamma-band activity exhibited a spatial distribution distinct from that of the delta-beta bands. This phenomenon, which has not been previously reported in brain organoids, suggests early functional specialization. The propagation analysis of organoids using this technology has the potential to deepen our understanding of the relationship between tissue architecture and electrical activity patterns in brain organoids. Additionally, it could serve as a powerful tool for elucidating the local effects of pharmacological compounds on neural circuits and uncovering the spatial features of neural circuits in disease models.

Data availability statement

The original contributions presented in this study are included in this article/Supplementary material, further inquiries can be directed to the corresponding author.

Author contributions

RY: Resources, Funding acquisition, Software, Formal analysis, Writing – review & editing, Data curation, Writing – original draft, Methodology, Conceptualization, Investigation, Visualization. NM: Methodology, Writing – review & editing, Visualization, Software, Formal analysis. YI: Software, Visualization, Methodology, Writing – review & editing, Formal analysis. IS: Project administration, Conceptualization, Funding acquisition, Visualization, Resources, Writing – original draft, Supervision, Writing – review & editing, Investigation.

Funding

The author(s) declare that financial support was received for the research and/or publication of this article. This study was supported by the Japan Society for the Promotion of Science (JSPS) KAKENHI (grant numbers 23H03726 and 25K21561) and a collaboration research grant with Sony Semiconductor Solutions Inc. The funder was not involved in the study design, collection, analysis, interpretation of data, the writing of this article, or the decision to submit it for publication.

Conflict of interest

IS is a founder of VitroVo, Inc., RY, NM and YI are also employees of VitoroVo. Inc.

Generative AI statement

The authors declare that no Generative AI was used in the creation of this manuscript.

Publisher's note

Supplementary material

The Supplementary Material for this article can be found online at: https://www.frontiersin.org/articles/10.3389/fnins.2025.1634582/full#supplementary-material

References

Andersen, J., Revah, O., Miura, Y., Thom, N., Amin, N. D., Kelley, K. W., et al. (2020). Generation of functional human 3D cortico-motor assembloids. *Cell* 183, 1913–1929.e26. doi: 10.1016/j.cell.2020.11.017

Başar, E. (2013). A review of gamma oscillations in healthy subjects and in cognitive impairment. *Int. J. Psychophysiol.* 90, 99–117. doi: 10.1016/j.ijpsycho.2013.07.005

Beaulieu, J. M., and Gainetdinov, R. R. (2011). The physiology, signaling, and pharmacology of dopamine receptors. *Pharmacol. Rev.* 63, 182–217. doi: 10.1124/pr.110.002642

Cardin, J. A., Carlén, M., Meletis, K., Knoblich, U., Zhang, F., Deisseroth, K., et al. (2009). Driving fast-spiking cells induces gamma rhythm and controls sensory responses. *Nature* 459, 663–667. doi: 10.1038/nature08002

Covelo, J., Camassa, A., Sanchez-Sanchez, J. M., Manasanch, A., Porta, L. D., Cancino-Fuentes, N., et al. (2025). Spatiotemporal network dynamics and structural correlates in the human cerebral cortex in vitro. *Prog. Neurobiol.* 246:102719. doi: 10.1016/j.pneurobio.2025.102719

Fukuda, M., Hata, Y., Ohshima, M., and Tsumoto, T. (1998). Role of NMDA receptors in the propagation of excitation in rat visual cortex as studied by optical imaging. *Neurosci. Res.* 31, 9–21. doi: 10.1016/S0168-0102(98)00018-2

Giandomenico, S. L., Sutcliffe, M., and Lancaster, M. A. (2021). Generation and long-term culture of advanced cerebral organoids for studying later stages of neural development. *Nat. Protoc.* 16, 579–602. doi: 10.1038/s41596-020-00433-w

Gonzalez, C., Armijo, E., Bravo-Alegria, J., Becerra-Calixto, A., Mays, C. E., and Soto, C. (2018). Modeling amyloid beta and tau pathology in human cerebral organoids. *Mol. Psychiatry* 23, 2363–2374. doi: 10.1038/s41380-018-0229-8

Guan, A., Wang, S., Huang, A., Qiu, C., Li, Y., Li, X., et al. (2022). The role of gamma oscillations in central nervous system diseases: Mechanism and treatment. *Front. Cell Neurosci.* 16:962957. doi: 10.3389/fncel.2022.962957

Herrmann, C. S., and Demiralp, T. (2005). Human EEG gamma oscillations in neuropsychiatric disorders. *Clin. Neurophysiol.* 116, 2719–2733. doi: 10.1016/j.clinph.2005.07.007

Homayoun, H., and Moghaddam, B. (2007). NMDA receptor hypofunction produces opposite effects on prefrontal cortex interneurons and pyramidal neurons. *J. Neurosci.* 27, 11496–11500. doi: 10.1523/jneurosci.2213-07.2007

Jo, J., Xiao, Y., Sun, A. X., Cukuroglu, E., Tran, H. D., Göke, J., et al. (2016). Midbrain-like organoids from human pluripotent stem cells contain functional dopaminergic and neuromelanin-producing neurons. *Cell Stem Cell* 19, 248–257. doi: 10.1016/j.stem.2016.07.005

Kato, Y., Matoba, Y., Honda, K., Ogawa, K., Shimizu, K., Maehara, M., et al. (2020). "High-density and large-scale MEA system featuring 236,880 electrodes at 11.72μm pitch for neuronal network analysis," in *Proceedings of the 2020 IEEE Symposium on VLSI Circuits*, (Honolulu), 1–2.

Kim, J.-I., Imaizumi, K., Jurjuţ, O., Kelley, K. W., Wang, D., Thete, M. V., et al. (2025). Human assembloid model of the ascending neural sensory pathway. *Nature* 642, 143–153. doi: 10.1038/s41586-025-08808-3

Lancaster, M. A., and Knoblich, J. A. (2014). Generation of cerebral organoids from human pluripotent stem cells. *Nat. Protoc.* 9, 2329–2340. doi: 10.1038/nprot.2014.158

Lancaster, M. A., Renner, M., Martin, C. A., Wenzel, D., Bicknell, L. S., Hurles, M. E., et al. (2013). Cerebral organoids model human brain development and microcephaly. *Nature* 501, 373–379. doi: 10.1038/nature12517

Li, Q., Clark, S., Lewis, D. V., and Wilson, W. A. (2002). NMDA receptor antagonists disinhibit rat posterior cingulate and retrosplenial cortices: A potential mechanism of neurotoxicity. *J. Neurosci.* 22, 3070–3080. doi: 10.1523/jneurosci.22-08-03070.2002

Lv, S., He, E., Luo, J., Liu, Y., Liang, W., Xu, S., et al. (2023). Using human-induced pluripotent stem cell derived neurons on microelectrode arrays to model neurological disease: A review. *Adv Sci.* 10:e2301828. doi: 10.1002/advs.202301828

Mariani, J., Coppola, G., Zhang, P., Abyzov, A., Provini, L., Tomasini, L., et al. (2015). FOXG1-dependent dysregulation of GABA/glutamate neuron differentiation in autism spectrum disorders. *Cell* 162, 375–390. doi: 10.1016/j.cell.2015.06.034

McNally, J. M., and McCarley, R. W. (2016). Gamma band oscillations: A key to understanding schizophrenia symptoms and neural circuit abnormalities. *Curr. Opin. Psychiatry* 29, 202–210. doi: 10.1097/yco.0000000000000244

Miura, Y., Li, M. Y., Birey, F., Ikeda, K., Revah, O., Thete, M. V., et al. (2020). Generation of human striatal organoids and cortico-striatal assembloids from human pluripotent stem cells. *Nat. Biotechnol.* 38, 1421–1430. doi: 10.1038/s41587-020-00763-w

Morales, M., and Root, D. H. (2014). Glutamate neurons within the midbrain dopamine regions. *Neuroscience* 282, 60–68. doi: 10.1016/j.neuroscience.2014.05.032

Morales-Villagrán, A., Ureña-Guerrero, M. E., and Tapia, R. (1996). Protection by NMDA receptor antagonists against seizures induced by intracerebral administration of 4-aminopyridine. *Eur. J. Pharmacol.* 305, 87–93. doi: 10.1016/0014-2999(96)00157-4

Notaras, M., Lodhi, A., Dündar, F., Collier, P., Sayles, N. M., Tilgner, H., et al. (2022). Schizophrenia is defined by cell-specific neuropathology and multiple neurodevelopmental mechanisms in patient-derived cerebral organoids. *Mol. Psychiatry* 27, 1416–1434. doi: 10.1038/s41380-021-01316-6

Ozgun, A., Lomboni, D. J., Aylsworth, A., Macdonald, A., Staines, W. A., Martina, M., et al. (2024). Unraveling the assembloid: Real-time monitoring of dopaminergic neurites in an inter-organoid pathway connecting midbrain and striatal regions. *Mater. Today Bio.* 25:100992. doi: 10.1016/j.mtbio.2024.100992

Pan, T., Jaklic, D. C., Vaid, S., Lin, G., VanHeyningen, D., and Dang, L. T. (2024). A multi-electrode array platform for modeling epilepsy using human pluripotent stem cell-derived brain assembloids. *J. Vis. Exp.* 211:e67396. doi: 10.3791/67396

Raja, W. K., Mungenast, A. E., Lin, Y. T., Ko, T., Abdurrob, F., Seo, J., et al. (2016). Self-organizing 3D human neural tissue derived from induced pluripotent stem cells recapitulate Alzheimer's disease phenotypes. *PLoS One* 11:e0161969. doi: 10.1371/journal.pone.0161969

Reumann, D., Krauditsch, C., Novatchkova, M., Sozzi, E., Wong, S. N., Zabolocki, M., et al. (2023). In vitro modeling of the human dopaminergic system using spatially arranged ventral midbrain-striatum-cortex assembloids. *Nat. Methods* 20, 2034–2047. doi: 10.1038/s41592-023-02080-x

Sakaguchi, H., Kadoshima, T., Soen, M., Narii, N., Ishida, Y., Ohgushi, M., et al. (2015). Generation of functional hippocampal neurons from self-organizing human embryonic stem cell-derived dorsomedial telencephalic tissue. *Nat. Commun.* 6:8896. doi: 10.1038/ncomms9896

Schröter, M., Wang, C., Terrigno, M., Hornauer, P., Huang, Z., Jagasia, R., et al. (2022). Functional imaging of brain organoids using high-density microelectrode arrays. *MRS Bull.* 47, 530–544. doi: 10.1557/s43577-022-00282-w

Sharf, T., van der Molen, T., Glasauer, S. M. K., Guzman, E., Buccino, A. P., Luna, G., et al. (2022). Functional neuronal circuitry and oscillatory dynamics in human brain organoids. *Nat. Commun.* 13:4403. doi: 10.1038/s41467-022-32115-4

Smirnova, L., Morales Pantoja, I. E., and Hartung, T. (2023). Organoid intelligence (OI) - The ultimate functionality of a brain microphysiological system. *Altex* 40, 191–203. doi: 10.14573/altex.2303261

Suzuki, I., Matsuda, N., Han, X., Noji, S., Shibata, M., Nagafuku, N., et al. (2023). Large-area field potential imaging having single neuron resolution using 236

880 electrodes CMOS-MEA Technology. *Adv. Sci.* 10:e2207732. doi: 10.1002/advs.202207732

Tasnim, K., and Liu, J. (2022). Emerging bioelectronics for brain organoid electrophysiology. *J. Mol. Biol.* 434:167165. doi: 10.1016/j.jmb.2021.167165

Trujillo, C. A., Gao, R., Negraes, P. D., Gu, J., Buchanan, J., Preissl, S., et al. (2019). Complex oscillatory waves emerging from cortical organoids model early human brain network development. *Cell Stem Cell* 25, 558–569.e7. doi: 10.1016/j.stem.2019.08.002

Yamaguchi, T., Sheen, W., and Morales, M. (2007). Glutamatergic neurons are present in the rat ventral tegmental area. *Eur. J. Neurosci.* 25, 106–118. doi: 10.1111/j.1460-9568.2006.05263.x

Yamaguchi, T., Wang, H. L., Li, X., Ng, T. H., and Morales, M. (2011). Mesocorticolimbic glutamatergic pathway. *J. Neurosci.* 31, 8476–8490. doi: 10.1523/jneurosci.1598-11.2011

Yan, Y., Song, L., Bejoy, J., Zhao, J., Kanekiyo, T., Bu, G., et al. (2018). Modeling neurodegenerative microenvironment using cortical organoids derived from human stem cells. *Tissue Eng. Part A* 24, 1125–1137. doi: 10.1089/ten.TEA.2017.0423

Yokoi, R., Nagafuku, N., Ishibashi, Y., Matsuda, N., and Suzuki, I. (2023). Contraindicated drug responses in dravet syndrome brain organoids utilizing micro electrode array assessment methods. *Organoids* 2, 177–191. doi: 10.3390/organoids2040014

Yokoi, R., Shibata, M., Odawara, A., Ishibashi, Y., Nagafuku, N., Matsuda, N., et al. (2021). Analysis of signal components < 500 Hz in brain organoids coupled to microelectrode arrays: A reliable test-bed for preclinical seizure liability assessment of drugs and screening of antiepileptic drugs. *Biochem. Biophys. Rep.* 28:101148. doi: 10.1016/j.bbrep.2021.101148